Appendix 3.6 – STRUCTURED GRIDS FROM EADS-MAS, GERMANY

by

Willy Fritz

A3.6.1 GEOMETRY

The test geometry is a delta wing with constant thickness, sharp trailing edge and different types of leading edges (sharp leading edge, small range leading edge radius, medium range leading edge radius and long range leading edge radius). The leading edge sweep angel is 65°. At the rear end of the wing there is a cylindrical sting which is blended by a fairing to the wing surface.

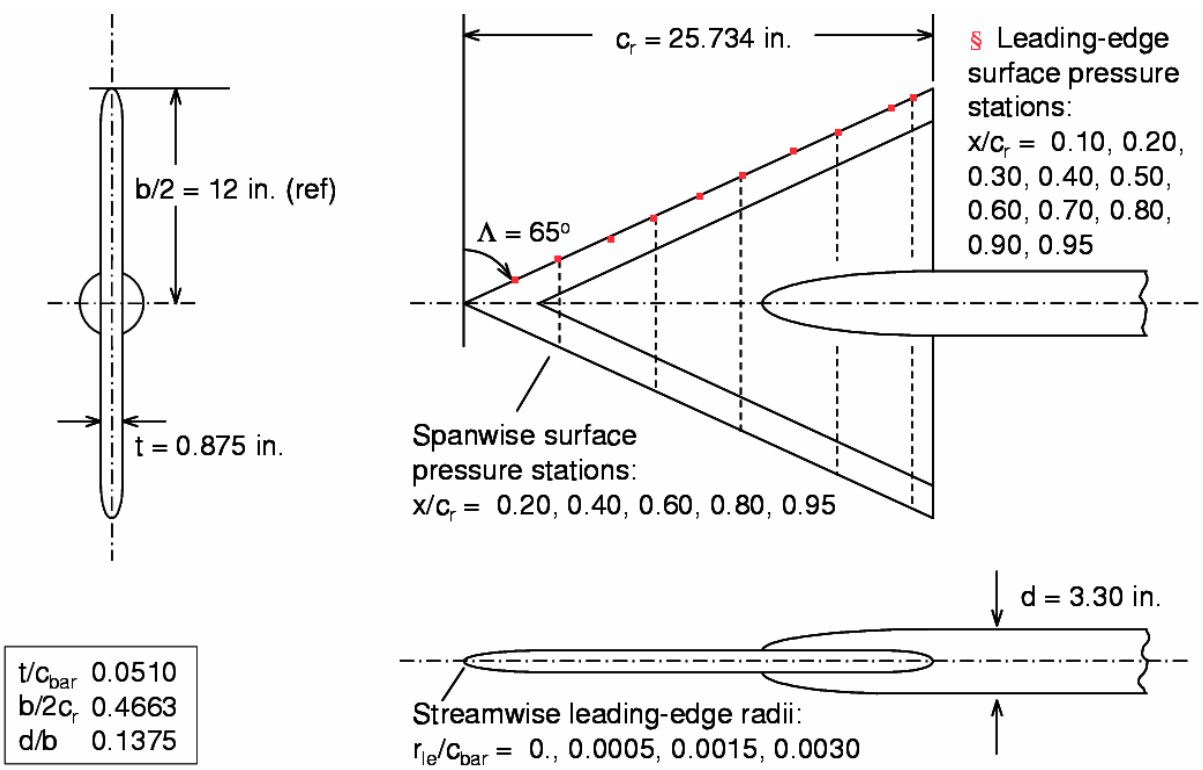

Figure A3.6-1: Geometry of VFE-2 Delta Wing.

Wing, sting-fairing and sting are analytically defined and this definition can be found in the NASA TM 465 (1996) "Julio Chu and James M. Luckring: Experimental Surface Pressure Data Obtained on 65° Delta Wing Across Reynolds Number and Mach Number Ranges, Volume 3: Medium Range Leading Edge". This report is on the NASA-LaRC techreports server http://techreports.larc.nasa.gov/ltrs/html available. To get the report and other publications concerning this delta wing type in the search-letters "Luckring Delta Wing".

A3.6.2 COMPUTATIONAL GRID

The computational grid is a so called conical grid having a singular line from the apex of the wing towards the upstream far field boundary. In the plane of symmetry, the grid wraps as a C-Mesh around the apex of the wing, in the cross sections x = const. the grid is of O-Type. The grid has been generated using a 3-D hyperbolic grid generator. The hyperbolic partial differential equations specify orthogonality and volume control. To avoid an intersection of the grid lines in concave corners (sting fairing) numerical dissipation is added to the equations.

The sting is included in the surface definition of the wing. This means, that the wing-sting intersection is not always mapped as an exact line in the grid. From the wing trailing edge, the sting is kept as a cylindrical body with constant cross section down to the far field boundary.

Figure A3.6-2 gives a total view of the 3-D grid structure. Figure A3.6-3 shows the grid in the plane of symmetry as well as the wing surface grid and the grid in the wake region. The conical grid (same number of grid points in each cross section x = const.) yields a very fine resolution of the apex of the wing.

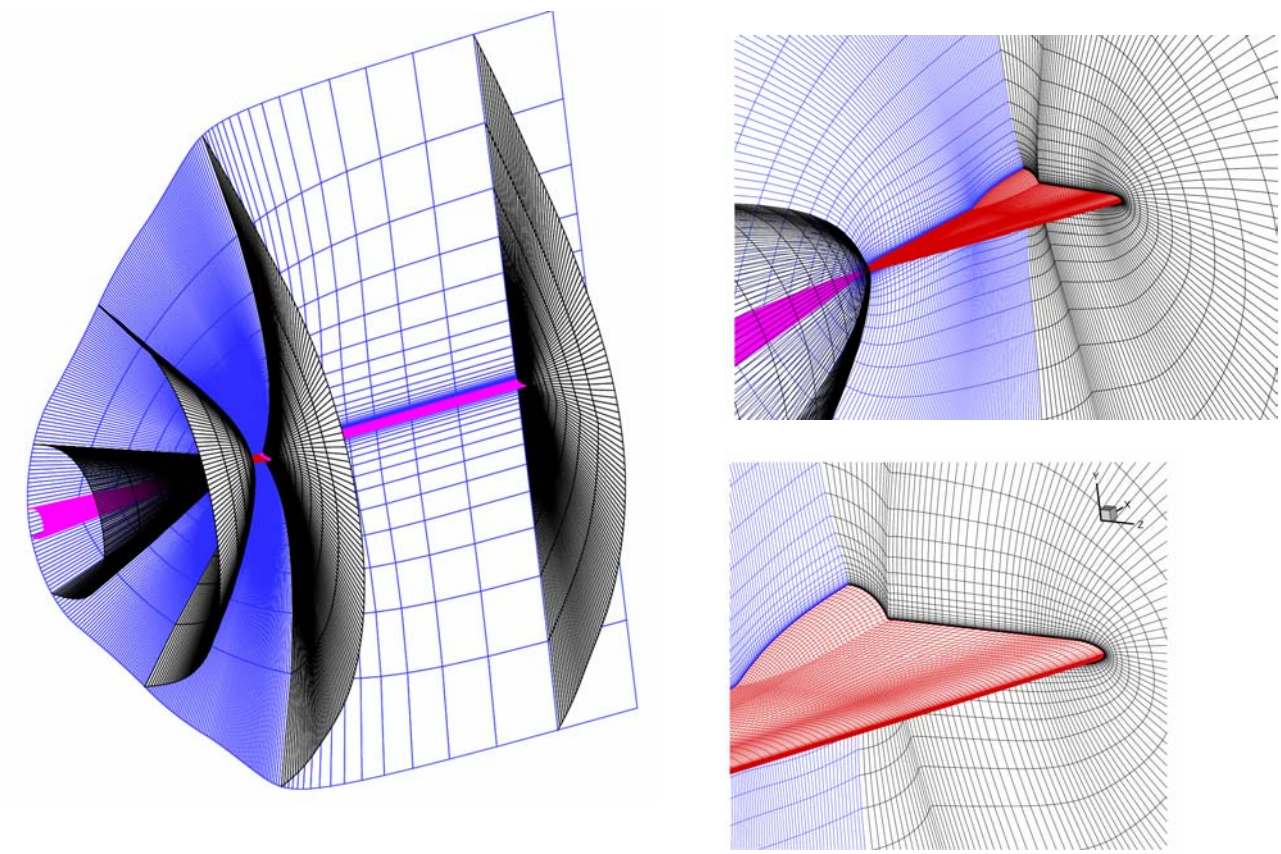

Figure A3.6-2: 3-D Grid Structure.

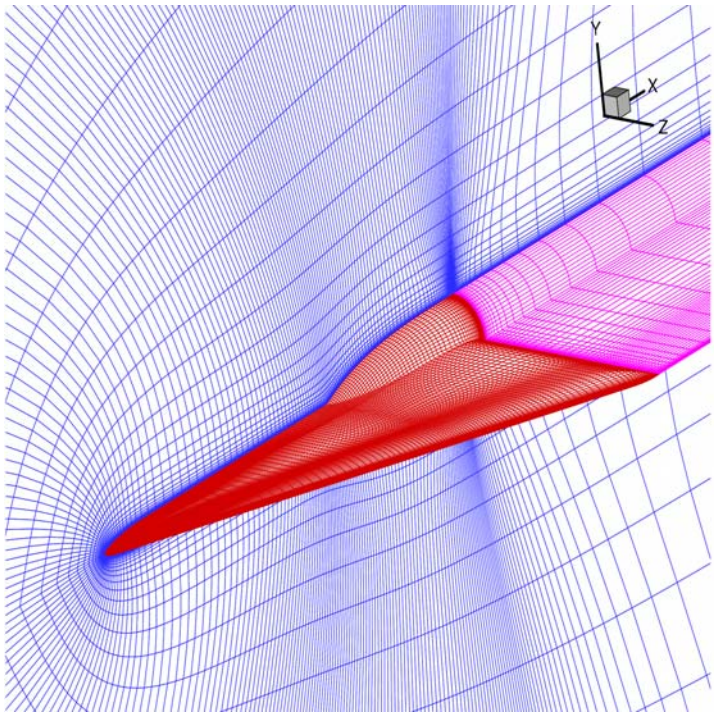

Figure A3.6-3: Grid in Plane of Symmetry.

Figure A3.6-4 shows the grid structure behind the wing. The O-mesh orientation of the last wing section is kept towards the far field boundary.

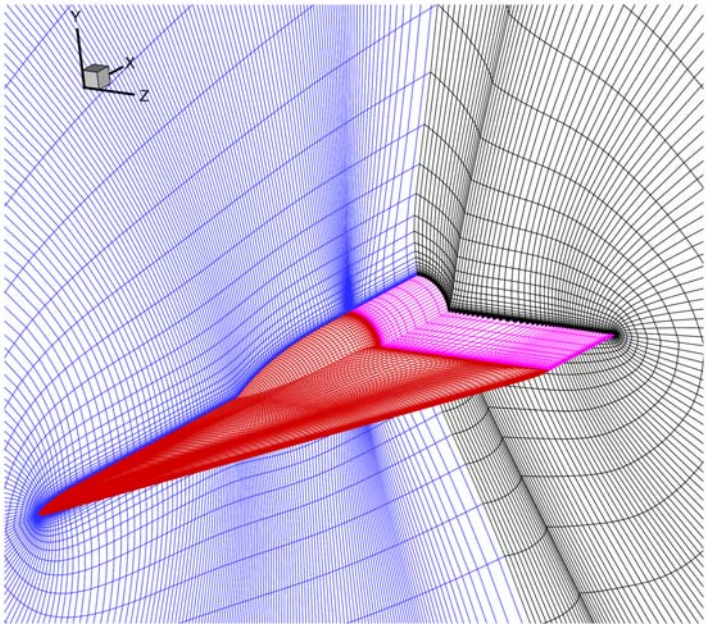

Figure A3.6-4: Grid Structure in Wake Region.

Figure A3.6-5 finally shows the grid lines around the leading edge. Due to the hyperbolic grid generation, the grid lines are nearly orthogonal around the leading edge.

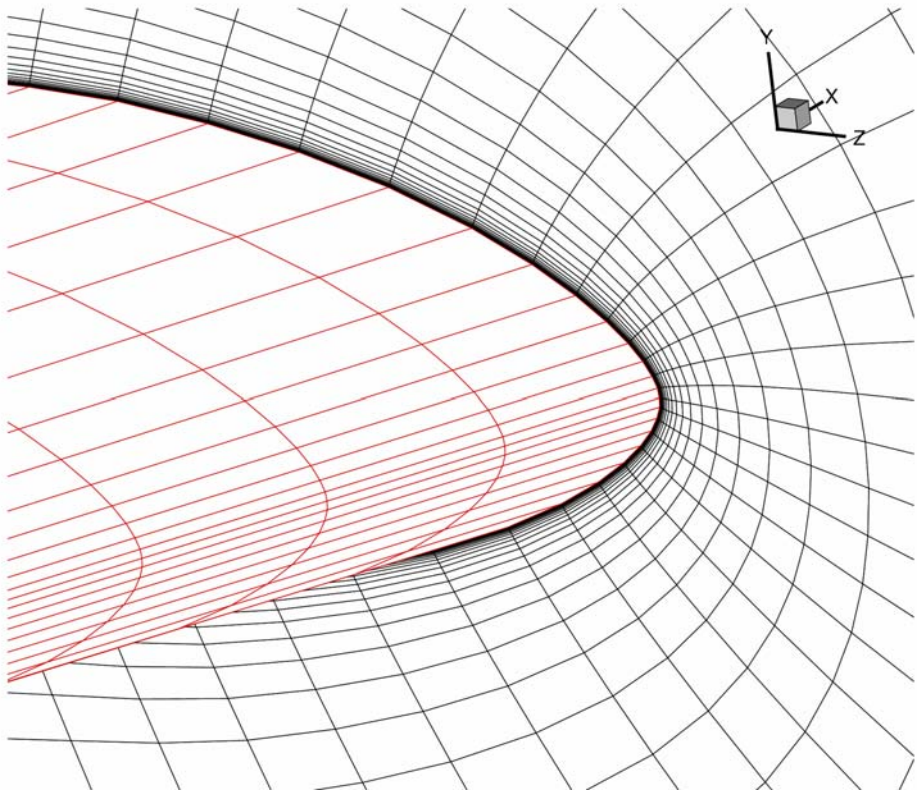

Figure A3.6-5: Grid around Leading Edge (only each second line is shown).

Two different grids have been generated fort he VFE-2 configuration:

Grid 1: 321*257*129 Points in i-, k- und j-direction.
Grid 2: 161*129*97 Points in i-, j- und k-direction.

This yields 10,642,113 points for grid 1 and 2,014,593 points for grid 2. The index directions are defined as follows:

i-direction: in stream wise direction, starting from the wing apex.
j-direction: from wing surface towards the far field.
k-direction: in span wise direction, beginning at the upper plane of symmetry and ending at the lower plane of symmetry.

Both grids cover only one half of the wing. The grids are so called single block grids. That means that the index space is one contiguous topological region. (Of course the grids can be subdivided into multiple blocks for parallel computations). Grid 1 is suitable for 5-level multi grid and grid 2 allows 4 level multi grid.

A3.6.3 AVAILABILITY OF THE GRIDS

Both grids are available as (compressed) ASCII-files as mono block grids. The grid data sets have been written by the following FORTRAN statements:

```
c
c
      write(21,'(a)') '$$  nblock  nlevel  icoord'
      write(21,'(4(i5,2x))') nblock,nlevel,icoord
c
      write(21,'(a,i5,a,i5)') '$$  block no.',nblck,' level no.',nlevel
      write(21,'(a)') '$$  physical block dimensions:'
      write(21,'(a)') '$$     i       j       k    iwidth'
      write(21,'(4(i5,2x))') il,jl,kl,iwidth
      write(21,'(a)') '$$  coordinates:'
      write(21,'(a)') '$$      x                y                z'
c
         do k =1,kl
            do j = 1,jl
               do i=1,il
                  write(21,'(3(e18.11, 1x))') x(i,j,k),y(i,j,k),z(i,j,k)
               end do
            end do
         end do
C
```

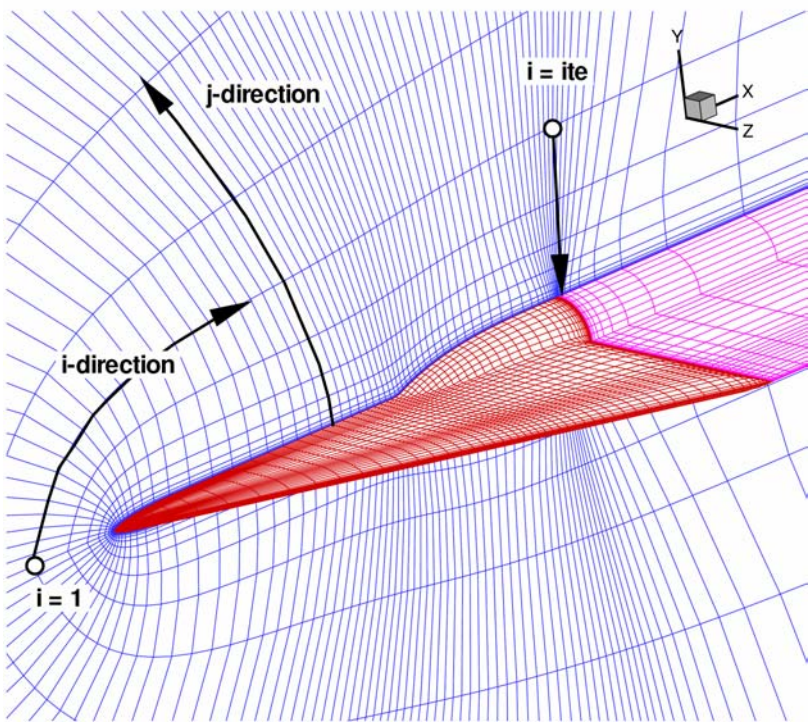

Figure A3.6-6: Index Directions i and j.

The coordinates are written within a multiple DO-Loop. The indices I, j and k are as described above Figure A3.6-6 and their orientation can be seen in the Figure A3.6-6, Figure A3.6-7 and Figure A3.6-8. These figures also show the orientation of the coordinate system. The origin is located in the apex of the wing.

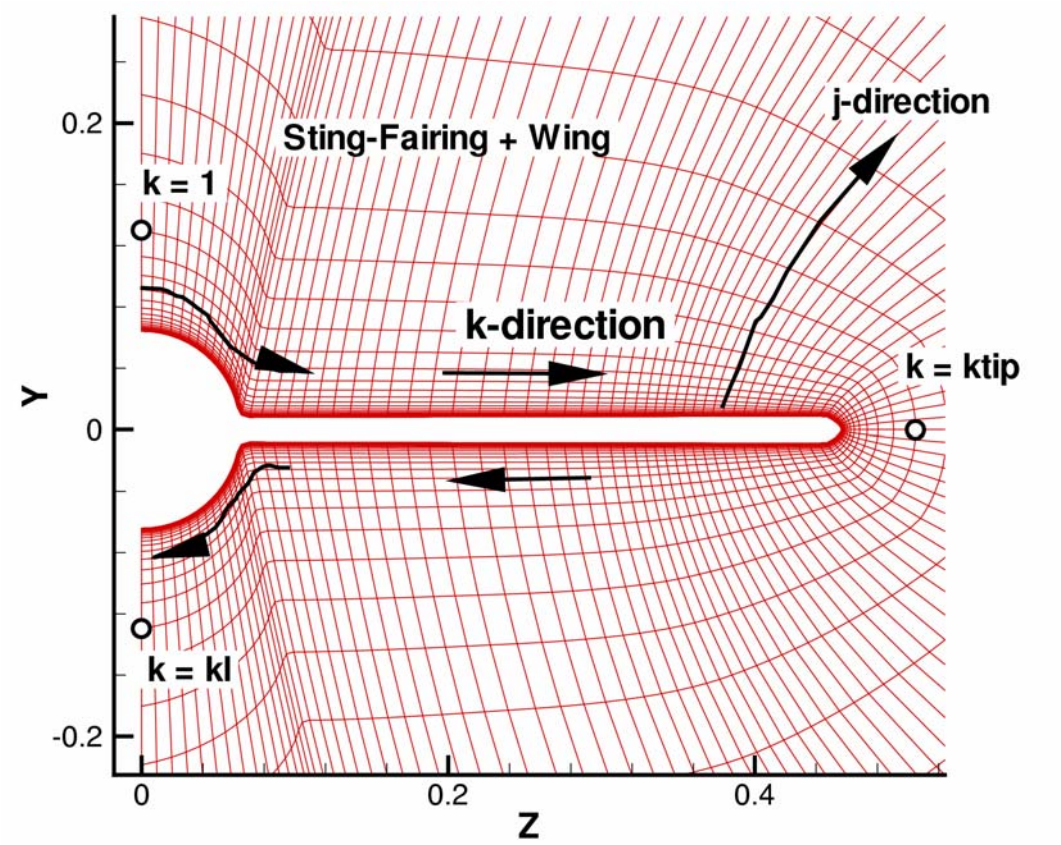

Figure A3.6-7: Index k in the Wing Region.

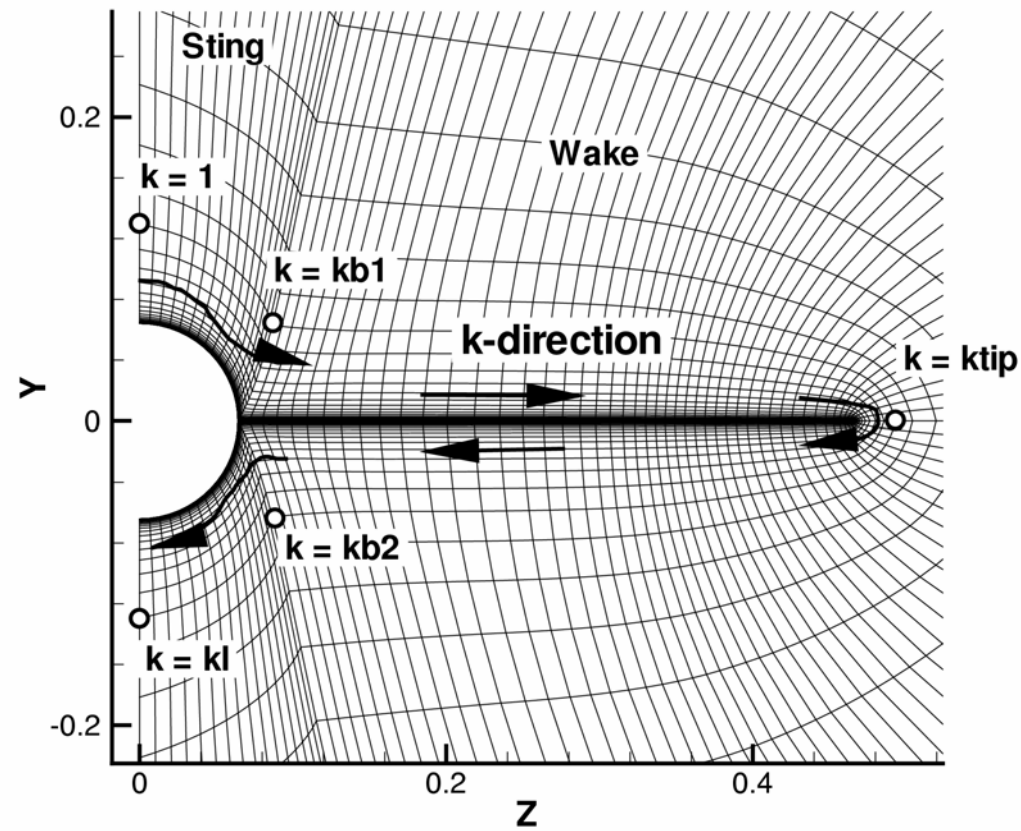

Figure A3.6-8: Orientation of Index k in the Wake Region.

The index I starts at the apex of the wing and runs in stream-wise direction towards the downstream far field (i = il). The wing trailing edge is located at i = ite. In the fine grid there is il = 321 and ite = 257, in grid 2 il = 161 and ite = 129.

The index k runs o-shaped around the configuration. From k = 1 to k = kl there is a solid wall as boundary condition. The location of the leading edge is ktip. In grid 1 kl = 257 and in grid 2 kl = 129. The index ktip is 129 in the fine grid and 65 in the medium grid.

In the wake region, there is a solid wall from k = 1 to k = kb1 and from k = kb2 to k = kl (sting). From k = kb1 over ktip to k = kb2 there is an internal cut in the flow field. For the fine grid (grid 1) kb1 = 33, and kb2 = 225, and in grid 2 kb1 = 17 and kb2 = 113.

The coordinates of all grids have been normalized with the wing root chord. This gives the following reference values:

c_r	= 1.0	
c_{mac}	= 0.6667	(Mean Aerodynamic Chord)
b/2	= 0.4663	(Halfspan)
S	= 0.23315	(Area of one half of the Wing)

As reference point fort he pitching moment xm = 0.5625 was used at EADS-MAS.

A3.6.4 SOME EADS RESULTS USING THE GRIDS

Following there are some results, which were obtained at EADS with these grids. All calculations were carried out using the DLR flow solver FLOWer 116.15 with the Wilcox k-ω turbulence model without transition setting.

Figure A3.6-9 shows the surface pressure contours in the medium grid for the DLR-test case (M = 0.4, Re = 3 million, α = 13°) without transition setting. There is a weak footprint of the second vortex. The main leading edge separation begins a little bit too late (this can be manipulated by setting transition.

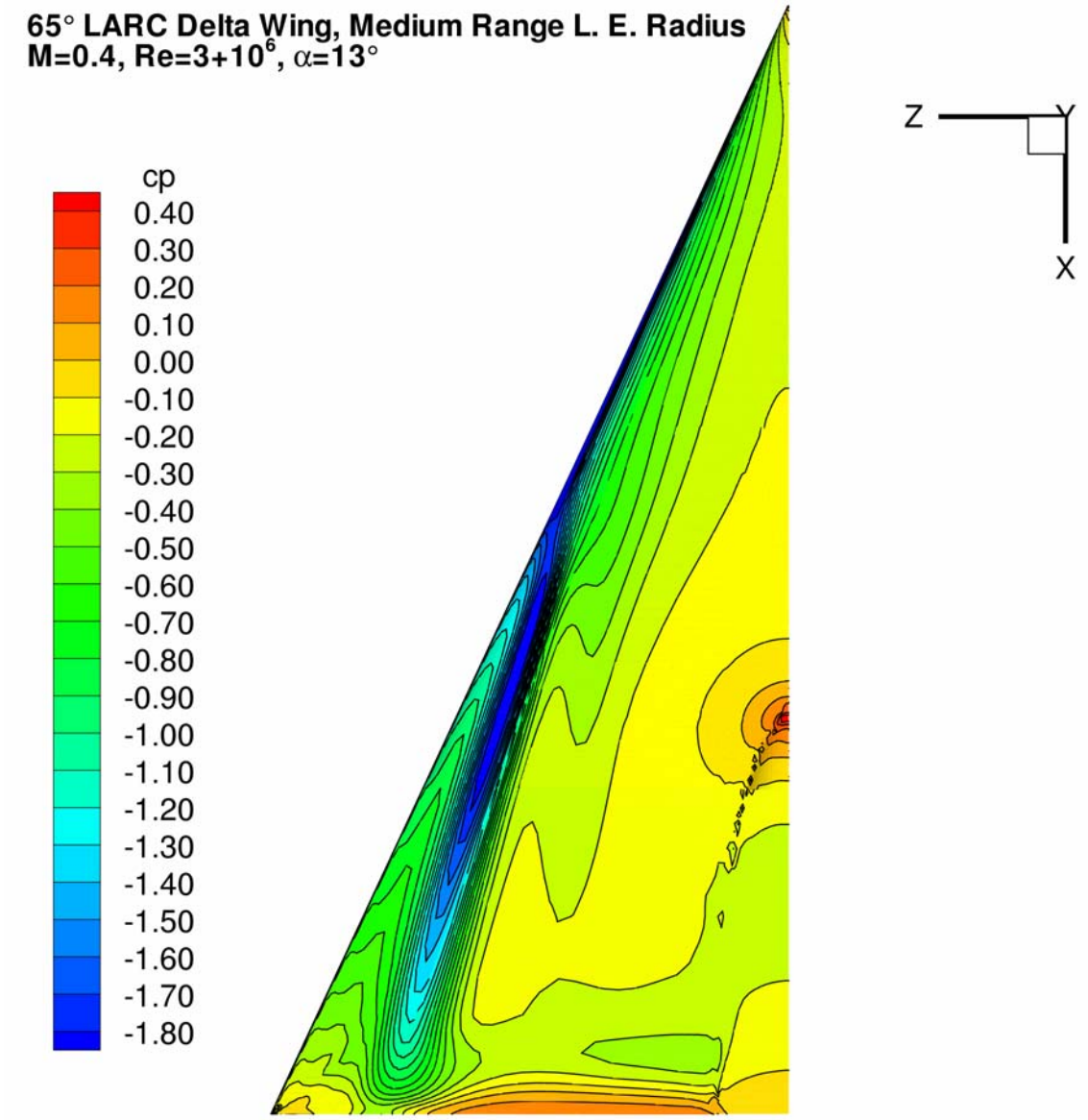

Figure A3.6-9: Surface Pressure Contours in Medium Grid.

Figure A3.6-10 shows the surface pressure contours for the same test case in the medium grid. The effect of the second vortex can be seen very clearly. But again the setup of the leading edge vortex separation is delayed compared to the experiment.

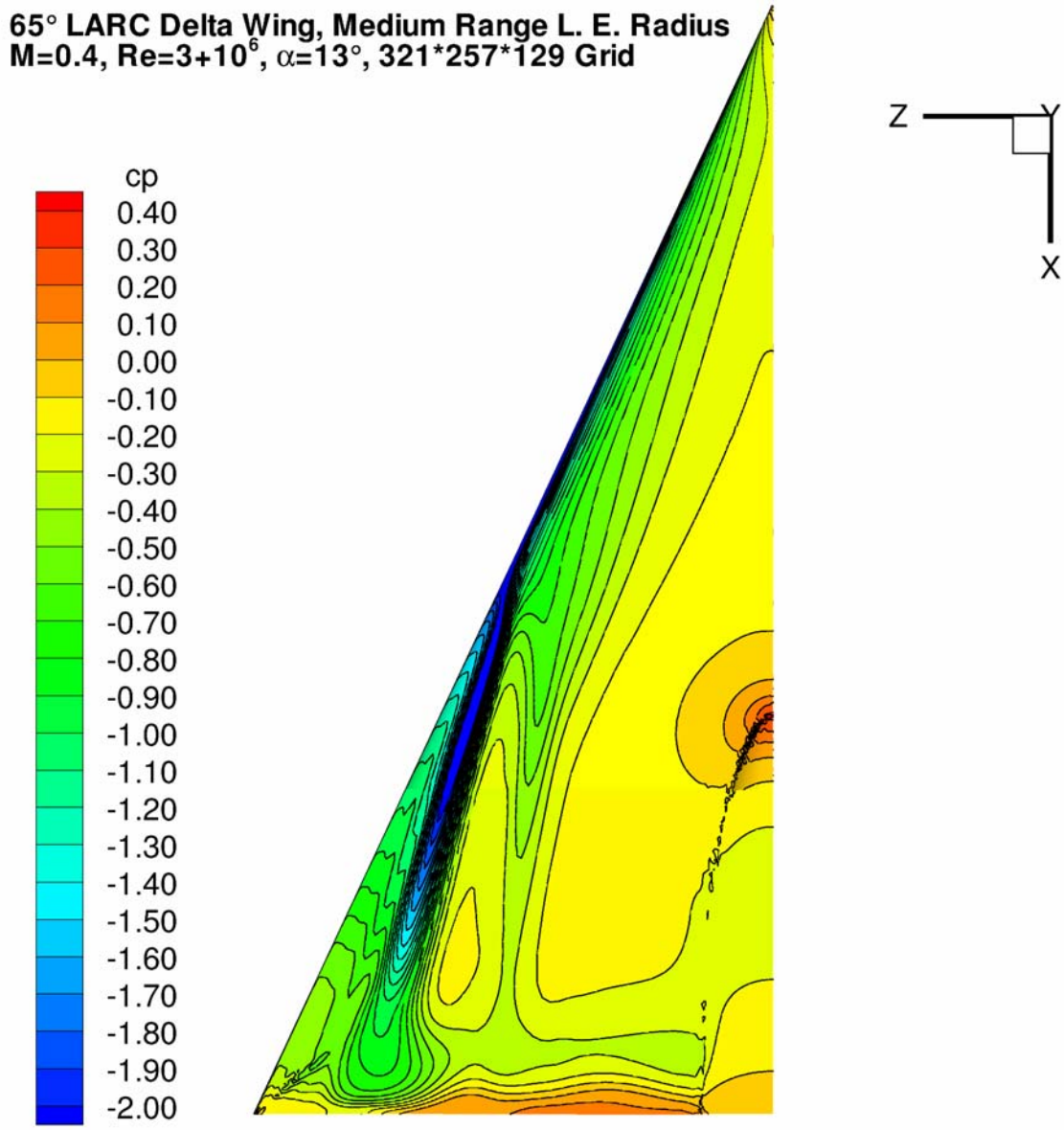

Figure A3.6-10: Pressure Contours in the Fine Grid.